Journal of Alloys and Compounds 509 (2011) 1411–1417

Contents lists available at ScienceDirect

Journal of Alloys and Compounds

journal homepage: www.elsevier.com/locate/jallcom

Near room temperature magnetic entropy changes in as-cast $Gd_{100-x}Mn_x$ (x = 0, 5, 10, 15, and 20 at.%) alloys

Tanjore V. Jayaraman [a,b,*], Laura Boone [a], Jeffrey E. Shield [a,b]

[a] Department of Mechanical Engineering, University of Nebraska, Lincoln, NE 68588, United States
[b] Nebraska Center for Materials and Nanoscience, University of Nebraska, Lincoln, NE 68588, United States

ARTICLE INFO

Article history:
Received 21 September 2010
Received in revised form 27 October 2010
Accepted 28 October 2010
Available online 10 November 2010

Keywords:
As-cast Gd–Mn alloys
Magnetocaloric
Magnetic entropy change
Refrigerant capacity

ABSTRACT

A series of $Gd_{100-x}Mn_x$ (x = 0, 5, 10, 15, and 20 at.%) alloys were prepared by arc-melting. The Curie temperature (T_C) associated with the ferromagnetic–paramagnetic transitions, derived from M–T curves, show decrease in T_C for as-cast alloys (~279 K) as compared to as-cast Gd (~292 K). No appreciable decrease in the $|\Delta S_M|_{max}$ values ~4.6 J/kg K (0–2 T) and ~8.6 J/kg K (0–5 T) were observed upon alloying Gd with Mn up to $x \leq 15$ at.%. Refrigerant capacity (q) showed negligible variation ~195 J/kg (0–2 T) and ~450 J/kg (0–5 T) with increasing Mn (up to $x \leq 15$ at.%) content. Similar values of $|\Delta S_M|_{max}$ and q coupled with ~13 K decrease in T_C for as-cast $Gd_{100-x}Mn_x$ ($0 \leq x \leq 15$) alloys as compared to Gd, suggests expansion of working temperature region of Gd upon alloying with Mn up to 15 at.%. Low cost, adjustable T_C, favorable magnetocaloric properties make $Gd_{100-x}Mn_x$ alloys potential candidates as second-order transition based magnetic refrigerants for near room temperature air-conditioning and magnetic refrigeration.

1. Introduction

The magnetocaloric effect (MCE) discovered by Warburg in 1881 in iron [1], displays itself in emission and absorption of heat by a magnetic material under the action of a magnetic field [2]. Under adiabatic conditions a magnetic field can cause cooling or heating of the material as a result of change in its internal energy. The term MCE is considered more widely in its application not only to the adiabatic temperature change (ΔT_{ad}) of a material but also to the isothermal magnetic entropy change ($|\Delta S_M|$) of its magnetic subsystem under the effect of the change in magnetic field (ΔH) [2–4]. The MCE often peaks at the Curie temperature (T_C). The MCE may be either measured directly or calculated indirectly from experimentally measured magnetization and/or heat capacity [4,5]. Practical application of the MCE is magnetic cooling or magnetic refrigeration. It has the potential to reduce the global energy consumption, eliminate the use of ozone-depleting compounds, greenhouse gases, and hazardous chemicals. Magnetic refrigeration near room temperature is of particular interest as it is an excellent alternative to vapor-compression refrigeration technology [3,6,7].

Large MCE (from cryogenic temperatures to room temperatures) have been observed in two kinds of magnetic materials: (a) materials that show a first-order transition (FOT) where a simultaneous structural and magnetic transition leads to a giant magnetic entropy change across its ordering temperature, viz. $FeMnP_{0.45}As_{0.55}$, $Gd_5Si_2Ge_2$ and so on [7–10]; (b) materials that show a second-order transition (SOT) where only a magnetic transition leads to magnetic entropy change across its ordering temperature, viz. few rare earth metals and their alloys, rare earth intermetallic compounds, few transition metal intermetallic compounds and some perovskites [6]. Giant magnetic entropy change in FOT materials is accompanied by large thermal and magnetic hysteresis losses, and they have a narrow working temperature range. These traits bring difficulties to their practical application and hence reduction in the magnetic refrigeration efficiency [11]. However the SOT materials, although their magnetic entropy changes are not as large, have reduced magnetic hysteresis, no thermal hysteresis and comparatively broader working temperature range. Additionally the time required for one refrigeration cycle for SOT material is lesser than the FOT materials owing to larger time required for simultaneous magnetic and structural transition in FOT materials. This becomes more pronounced when the operation of a magnetic refrigeration process involves numerous refrigeration cycles. Most of the current research interests are focused on either depressing the magnetic hysteresis in FOT materials or improving MCE (ΔT_{ad} or $|\Delta S_M|$) in SOT materials. Developing suitable SOT-based magnetic materials, which display large MCE near room temperature and can be operated in magnetic fields ~2 T or less, generated by permanent magnets, are of particular interest [11–13].

The rare earth metal Gd is a popular SOT magnetic refrigerant for the room temperature magnetic refrigerator. Some of its alloys are considered to be a potential magnetic refrigerant for air condi-

* Corresponding author. Tel.: +1 402 472 9371.
E-mail addresses: tjayaraman2@unl.edu, tvjayaraman@gmail.com (T.V. Jayaraman).

0925-8388/$ – see front matter © 2010 Elsevier B.V. All rights reserved.
doi:10.1016/j.jallcom.2010.10.208

tioning and refrigeration near room temperature [3,4]. The cooling efficiency in magnetic refrigerators working with Gd was shown to reach 60% of the theoretical limit compared to only about 40% in the best vapor compression refrigerators [14]. Considering the various requirements for practical application, it is necessary to search for magnetic refrigerants possessing MCE (ΔT_{ad} or $|\Delta S_M|$) as good as Gd, and have near room temperature T_C (~298 ± 30 K). In order to alter T_C (increase the working temperature range) and increase the maximum magnetic entropy change ($|\Delta S_M|_{max}$), in the past many binary Gd-based alloys have been studied. The conventionally melted binary Gd–R (R = lanthanide elements such as Dy, Ho, Tb, and Yb) alloys have both T_C and $|\Delta S_M|_{max}$ less than that of Gd [2,7]. For the binary Gd–T (T = transition elements such as Ag, Co, V, Y, Zn) alloys T_C decreases with alloying; $|\Delta S_M|_{max}$ decreases for rapidly solidified Gd–Ag and conventionally melted Gd–Zn alloys; it remains constant for melt-spun Gd–Co and as-cast Gd–Y alloys; and increases for as-cast Gd–V alloys as compared to Gd. Few Gd–T (T = V, Y) alloys have higher refrigeration capacity (q) and relative cooling power (RCE) as compared to Gd [12,15–18]. Studies in conventionally melted binary Gd–X (X = B, C) alloys show slight increase in T_C and decrease in $|\Delta S_M|_{max}$ upon alloying Gd with B or C [19–21]. Hydrogen-doped Gd (GdH_x) shows enhancement in both T_C and $|\Delta S_M|_{max}$ [22]. Studies on the Laves compounds $Gd(Fe,Al)_2$ show rapid decrease in $|\Delta S_M|_{max}$ compared with Gd, and T_C reduces to ~265 K [23]. The Laves phase $GdMn_2$ also shows rapid decrease in $|\Delta S_M|_{max}$ compared with Gd; however, it is not suitable for room temperature applications (T_C ~ 35 K and T_N ~ 105 K) [24,25].

Based on the past work reported in the literature, the effect of binary alloying with a few of the transition metals in Period 4 of the modern periodic table (V, Co and Zn) on the MCE of Gd reveals the following: binary alloying of these metals with Gd decreases the T_C of the respective alloys of Gd [12,16,17]. However the effect of binary alloying of these elements with Gd on $|\Delta S_M|_{max}$ is interesting: binary alloying of V($[Ar]3d^34s^2$), which is paramagnetic, increases $|\Delta S_M|_{max}$ in conventionally melted Gd–V alloys [17]; $|\Delta S_M|_{max}$ remains constant for melt-spun Gd–Co alloys upon alloying with ferromagnetic Co($[Ar]3d^74s^2$) [12]; and, while binary alloying with Zn ($[Ar]3d^{10}4s^2$), which is diamagnetic, decreases $|\Delta S_M|_{max}$ in conventionally melted-cast Gd–Zn alloys [16]. It would be interesting to know how Mn ($[Ar]3d^54s^2$), which is paramagnetic and lies in between V and Co (also less expensive than V and Co) in, Period 4, would influence $|\Delta S_M|_{max}$ and T_C upon its alloying with Gd to form Gd–Mn alloys. To date there is no research that we are aware of, in the literature regarding MCE of binary Gd–Mn alloys.

Fig. 1 shows the Gd-rich part of the Gd–Mn binary equilibrium phase diagram [26,27]. Mn has negligible solubility in Gd at all temperatures. A eutectic reaction occurs at 830 °C (at 35.5 at.% Mn) where upon cooling through the eutectic temperature, the lowest melting liquid of the system, decomposes to two solid phases, α-Gd and $GdMn_2$. The α-Gd crystallizes in the hexagonal A3 phase (*hP2* Pearson symbol, *P6₃/mmc* space group, Mg-type structure) while $GdMn_2$ crystallizes in the cubic C15 Laves phase (*cF24* Pearson symbol, *Fd3m* space group, $MgCu_2$-type structure) [24–28]. In regard to their magnetic properties, α-Gd is ferromagnetic and undergoes magnetic transition ferromagnetic to paramagnetic at ~293 K [3–8]. $GdMn_2$ exhibits interesting magnetic properties due to the existence of two magnetic sublattices. It presents a first-order antiferromagnetic transitions at T_N (Neel temperature) ~108 K related with the magnetic ordering of the Gd ions. Few works have suggested that the Gd sublattice also orders at 108 K together with the Mn moments, and therefore the low-temperature transition could be considered as a spin re-orientation temperature [25,28].

In this paper we report the magnetocaloric properties of as-cast $Gd_{100-x}Mn_x$ (x = 0, 5, 10, 15, and 20 at.%) alloys at near room temperature (250–320 K). This study could give light into some aspects of alloy design strategy that needs to be adopted that could auger in the development of superior SOT materials based on Gd-alloys having improved MCE properties suitable for practical application in near-room temperature magnetic refrigeration.

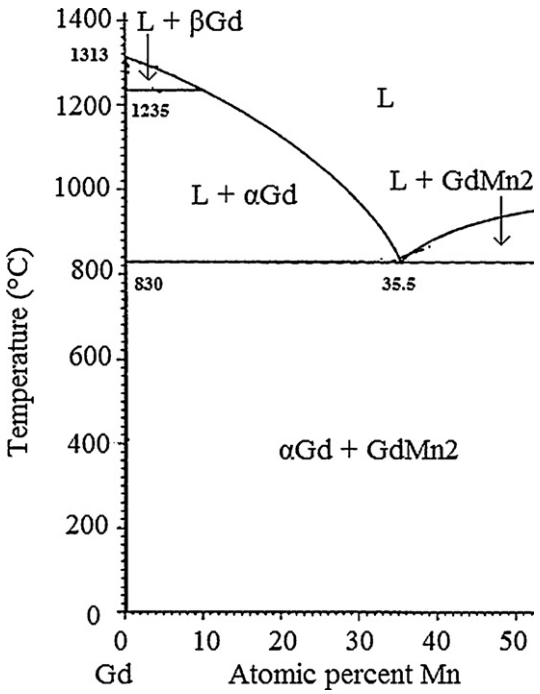

Fig. 1. The Gd-rich portion of Gd–Mn equilibrium phase diagram. Adapted from [26].

2. Experimental details

2.1. Alloy preparation

The nominal composition of $Gd_{100-x}Mn_x$ (x = 0, 5, 10, 15, and 20 at.%) alloy ingots was prepared from high purity (>99.95%) elemental constituents (Gd and Mn) by arc-melting. The melting of the alloys was performed in an ultra-high-purity argon atmosphere. Each of the alloys was re-melted five times to ensure compositional homogeneity. The energy dispersive X-ray (EDX) analysis showed the composition of the alloys varied within ±1.2 at.% of their respective nominal composition.

2.2. X-ray characterization, optical metallography and microhardness measurements

The as-cast alloys were analyzed by a Rigaku MultiFlex X-ray diffractometer with θ–θ geometry using Cu Kα radiation. Optical metallography of the alloys was performed using Leica DM 2500 microscope. Metallographic samples of each of the alloys were polished down to 0.3 μm alumina to obtain smooth surface relatively free of scratch. Metallographic etching was performed using various etchants suggested for Gd-based alloys [29]. However after numerous iterations with various etchants the ~0.5% Nital etchant (199 mL ethanol 96% + 1 mL nitric acid 65%) with etching time of 10–15 s was found to be optimum for etching of as-cast $Gd_{100-x}Mn_x$ (x = 5, 10, 15, and 20 at.%) alloys. The Vickers microhardness was measured using a Wilson Tukon Series 200 microhardness tester in accordance to the ASTM Standard Test Method for Micro-indentation Hardness of Materials (ASTM E 384-99) [30].

2.3. Magnetic characterization

The magnetic characterization was performed using Quantum Design, Magnetic Property Measurement System (MPMS-XL) magnetometer in fields up to 5 T over a temperature range of 100–320 K. The accuracy of temperature measurement was within ±0.2 °C and that for magnetization measurement was within ±1%. The entropy change resulting from the spin-ordering, induced by applied magnetic field (H), depends on the temperature gradient of magnetization (M) and can be obtained from Maxwell's thermodynamic relation:

$$\left|\frac{\partial S(T,H)}{\partial H}\right|_T = \left|\frac{\partial M(T,H)}{\partial T}\right|_H \quad (1)$$

after integrating with respect to the applied field strength H, in accordance with the thermodynamic relation [4]:

$$\Delta S_M(T,H) = S_M(T,0) - S_M(T,H) = \int_0^{\Delta H} \left(\frac{\partial M(T,H)}{\partial T}\right)_{dH} \quad (2)$$

In the present study for each of the alloys, M–T curves were obtained at different H (0–5 T). From the $(M$–$T)_H$ data the $(\partial M/\partial T) - H$ plots for various temperatures (250–320 K) were generated. Finally by integrating such a plot up to the desired field value H (0–2 T, 0–5 T), the magnetic entropy change in the sample due to the applied field H (2 T, 5 T) as a function of temperature T was determined.

The magnetic entropy change of a solid directly characterizes the refrigeration capacity (cooling capacity), q of a magnetic refrigerant. By performing a numerical integration to evaluate the area subtended by the peaks in $\Delta S_M - T$ plots, q, defined as

$$q = \int_{T1}^{T2} \left|\Delta S_M(T,\Delta H)\right| dT \quad (3)$$

can be obtained. Here T_1 and T_2 are the temperature of the cold and hot sinks, respectively. It is a measure of how much heat can be transferred between the cold and the hot sink in one ideal refrigeration cycle. In other words when two different materials are used in the same refrigeration device, the material with higher refrigeration capacity is expected to perform better since it will support the transfer of greater amount of heat in a real cycle provided all parameters of the magnetic refrigerator remain the same [2,4,31].

3. Results and discussion

Fig. 2 shows the X-ray diffraction spectra for as-cast $Gd_{100-x}Mn_x$ (x = 0, 5, 10, 15, and 20 at.%) alloys. The as-cast Gd (Mn-free) is comprised of hcp α-Gd. The equilibrium phase diagram (Fig. 1) of binary Gd–Mn alloys, predicts the presence of $GdMn_2$ phase along with α-Gd phase for $Gd_{95}Mn_5$ alloy, cooled under equilibrium conditions. However the X-ray diffraction spectra show the presence of hcp α-Gd phase and absence of $GdMn_2$ phase for as-cast $Gd_{95}Mn_5$ alloy. This could be attributed due to either the formation of $GdMn_2$ phase is suppressed owing to relatively faster cooling during the preparation of the as-cast alloy during arc-melting as compared to equilibrium cooling or the amount of $GdMn_2$ phase formed in the alloy is less than the detection limits of X-ray diffraction (~3–5%). The presence or absence of $GdMn_2$ phase in the as-cast $Gd_{95}Mn_5$ alloy could be confirmed by metallographic characterization of these alloys. However the X-ray diffraction spectra show the presence of both α-Gd phase and $GdMn_2$ phase for as-cast $Gd_{90}Mn_{10}$, $Gd_{85}Mn_{15}$, $Gd_{80}Mn_{20}$ alloys. The presence of $GdMn_2$ phase in these alloys can be inferred from the emergence of (3 1 1) peak of $GdMn_2$ at $2\theta \sim 38.5^\circ$. The other prominent peaks of $GdMn_2$ viz. (2 2 0) at $2\theta \sim 32.5^\circ$ and (3 3 3) at $2\theta \sim 62^\circ$ coincide with the peaks of α-Gd phase viz. (1 0 1) at $2\theta \sim 32.5^\circ$ and (2 0 1) at $2\theta \sim 62^\circ$, respectively and hence the emergence of these peaks may not be inferred so clearly from the X-ray diffraction spectra of α-Gd phase.

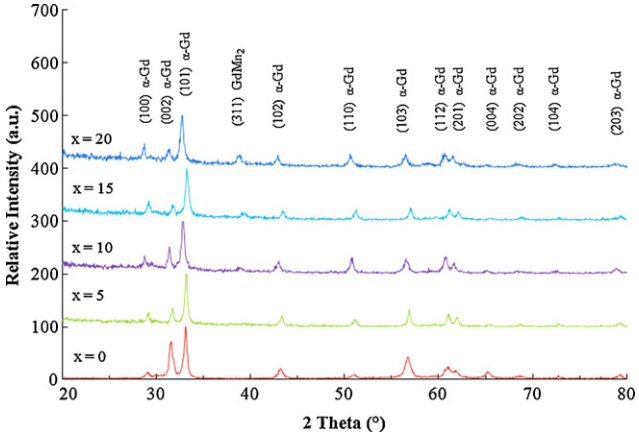

Fig. 2. X-ray spectra of as-cast $Gd_{100-x}Mn_x$ (x = 0, 5, 10, 15, 20 at.%) alloys.

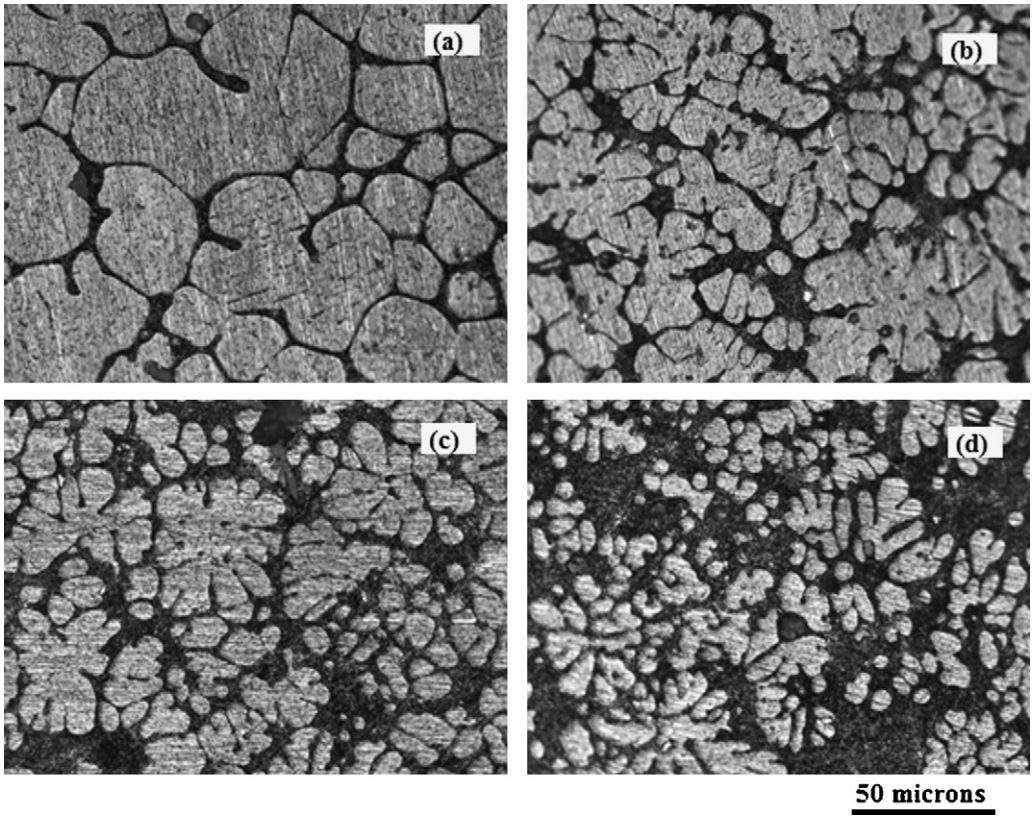

Fig. 3. The optical micrographs of as-cast $Gd_{100-x}Mn_x$ (x = 5, 10, 15, 20 at.%) alloys; (a) $Gd_{95}Mn_5$, (b) $Gd_{90}Mn_{10}$, (c) $Gd_{85}Mn_{15}$, and (d) $Gd_{80}Mn_{20}$.

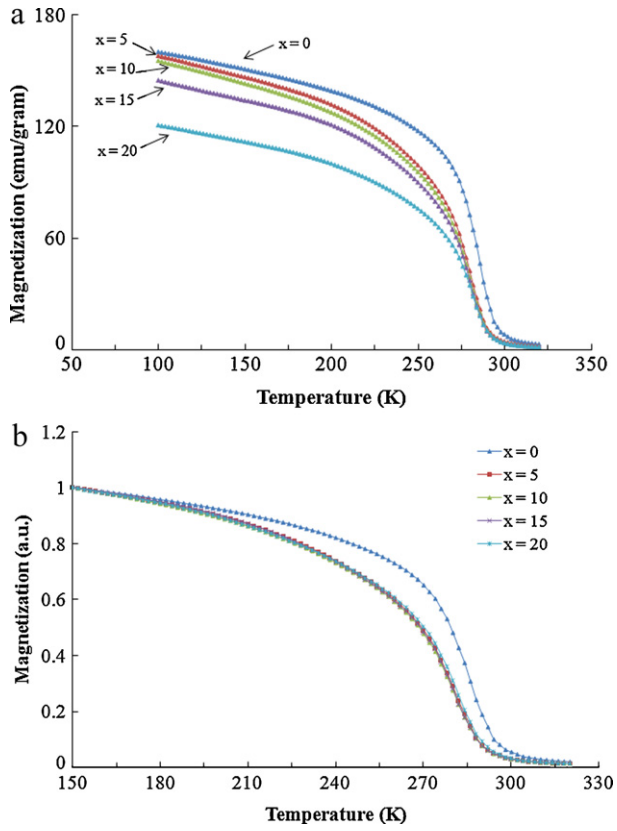

Fig. 4. (a) The temperature dependence of magnetization in a field of 0.1 T for as-cast $Gd_{100-x}Mn_x$ (x = 0, 5, 10, 15, 20 at.%) alloys and (b) magnetization curves normalized to unity at 150 K.

In order to confirm the presence/absence of $GdMn_2$ phase in as-cast $Gd_{95}Mn_5$ alloy the optical microstructural characterization of the as-cast $Gd_{100-x}Mn_x$ alloys was performed. Fig. 3 shows the optical micrograph of the as-cast $Gd_{100-x}Mn_x$ (x = 5, 10, 15, and 20 at.%) alloys. From the microstructure the presence of $GdMn_2$ phase in as-cast $Gd_{95}Mn_5$ alloy was confirmed. The light region with large grains (~40 μm) corresponds to α-Gd phase (pro-eutectic). The dark region along some portions of the grain boundary of the pro-eutectic α-Gd phase and at the junctions of two or more of their grains (triple points) corresponds to eutectic phase (α-Gd + $GdMn_2$). In the microstructure of as-cast $Gd_{95}Mn_5$, $Gd_{90}Mn_{10}$, $Gd_{85}Mn_{15}$ and $Gd_{80}Mn_{20}$ alloys one can distinctively observe increasing amount of darker regions (eutectic α-Gd + $GdMn_2$ phase) and decreasing amount of islands of dendrites of pro-eutectic α-Gd phase with the increase in Mn content.

The temperature dependence of magnetization for the as-cast $Gd_{100-x}Mn_x$ (x = 5, 10, 15, and 20 at.%) alloys measured in a magnetic field of 0.1 T is shown in Fig. 4. The T_C for the as-cast alloys, determined from the M–T curves by inflexion method [4], i.e. temperature where $\left|\partial M/\partial T\right|$ is maximum, is listed in Table 1. The T_C for as-cast Gd is 292.2 K. This agrees closely with the previously

Table 1
The Curie temperature (T_C), maximum magnetic entropy change ($|S_M|_{max}$) and refrigerant capacity (q) of as-cast $Gd_{100-x}Mn_x$ (x = 0, 5, 10, 15, 20 at.%) alloys.

As-cast alloy	T_C (K)	$\|\Delta S_M\|_{max}$ (J/kg K) (0–2 T)	q (J/kg) (0–2 T)	$\|\Delta S_M\|_{max}$ (J/kg K) (0–5 T)	q (J/kg) (0–5 T)
Gd	292.2	4.77	198	8.92	461
$Gd_{95}Mn_5$	279.9	4.69	202	8.83	467
$Gd_{90}Mn_{10}$	279.1	4.54	196	8.52	454
$Gd_{85}Mn_{15}$	278.9	4.41	190	8.38	425
$Gd_{80}Mn_{20}$	279.9	3.67	163	7.10	376

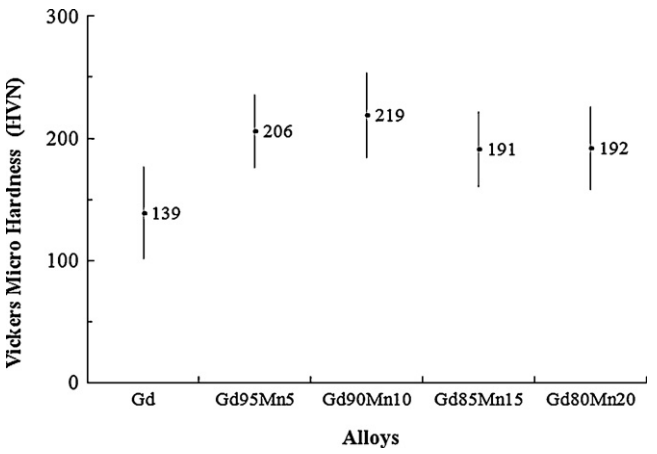

Fig. 5. The dependence of Vickers MicroHardness (HVN) of α-Gd phase on the composition of Mn for as-cast $Gd_{100-x}Mn_x$ (x = 0, 5, 10, 15, 20 at.%) alloys.

reported T_C values (~293 K) for Gd [3–8]. T_C of Gd is very sensitive to its purity level [1–10]. Minor difference (~1 K) in the T_C obtained for as-cast Gd as compared to previously reported T_C values for Gd could be due to the purity levels between Gd used in the current study and previous studies. As-cast Gd upon heating in the vicinity of its T_C, the magnetization decreases rapidly owing to magnetic transition in α-Gd from ferromagnetism to paramagnetism. For as-cast $Gd_{95}Mn_5$ alloy the T_C is 279.9 K. There is a decrease in T_C by ~12 K with the addition of 5 at.% Mn to Gd. However with further addition of Mn to Gd, the T_C values for as-cast $Gd_{90}Mn_{10}$, $Gd_{85}Mn_{15}$, and $Gd_{80}Mn_{20}$ alloys remains close to ~279 K. In the as-cast alloys which are comprised of both α-Gd and $GdMn_2$ phase, the rapid decrease in magnetization in the vicinity of their respective T_C is attributed only to the magnetic transition in α-Gd phase from ferromagnetism to paramagnetism. It may be noted that $GdMn_2$ phase undergoes first-order anti-ferromagnetic transition at a very low temperature (T_N ~ 108 K) [28] and hence its contribution to the magnetization can be expected to be negligible. The as-cast alloys having lower T_C (~279 K) as compared to as-cast Gd (~292 K) could be attributed to a negligible amount of Mn that is dissolved in α-Gd, thus forming a substitutional solid solution. Similar values of T_C ~ 279 K for the as-cast alloys suggest the possibility that the amount of Mn dissolved in α-Gd in these alloys are of similar amount, as would be expected.

At any temperature below T_C (Fig. 4(a)) the magnetization of as-cast $Gd_{100-x}Mn_x$ alloys (x = 0, 5, 10, 15, 20) decreases with increase in Mn at.%. This is attributed to the decrease in the volume fraction of ferromagnetic α-Gd phase and increase in volume fraction of non-magnetic $GdMn_2$ phase. Fig. 4(b) shows the temperature dependence of magnetization ($M/M_{150\,K}$–T) in these alloys, where the magnetization of each of the alloy is normalized with their respective magnetization values at 150 K, so that the T_C and the variation of magnetization with increase in Mn addition may become intelligible. The overlapping of the curves for as-cast $Gd_{100-x}Mn_x$ (x = 5, 10, 15, 20) alloys suggests presence of similar amount of Mn in α-Gd phase irrespective of composition of Mn in the as-cast alloys.

The formation of substitutional solid solution of Mn in α-Gd phase in as-cast $Gd_{100-x}Mn_x$ (x = 5, 10, 15, 20) alloys was confirmed by measuring the Vickers microhardness number (HVN) in the grains of α-Gd phase in each of the as-cast alloys. The load used for micro-indentation was 25 gf and the HVN was measured at the center of each of the ~50 grains of α-Gd phase, selected randomly, for each alloy to obtain better statistics. Fig. 5 shows the variation of HVN for α-Gd phase in as-cast $Gd_{100-x}Mn_x$ (x = 0, 5, 10, 15, 20) alloys. The observed variation in HVN among grains of α-Gd phase

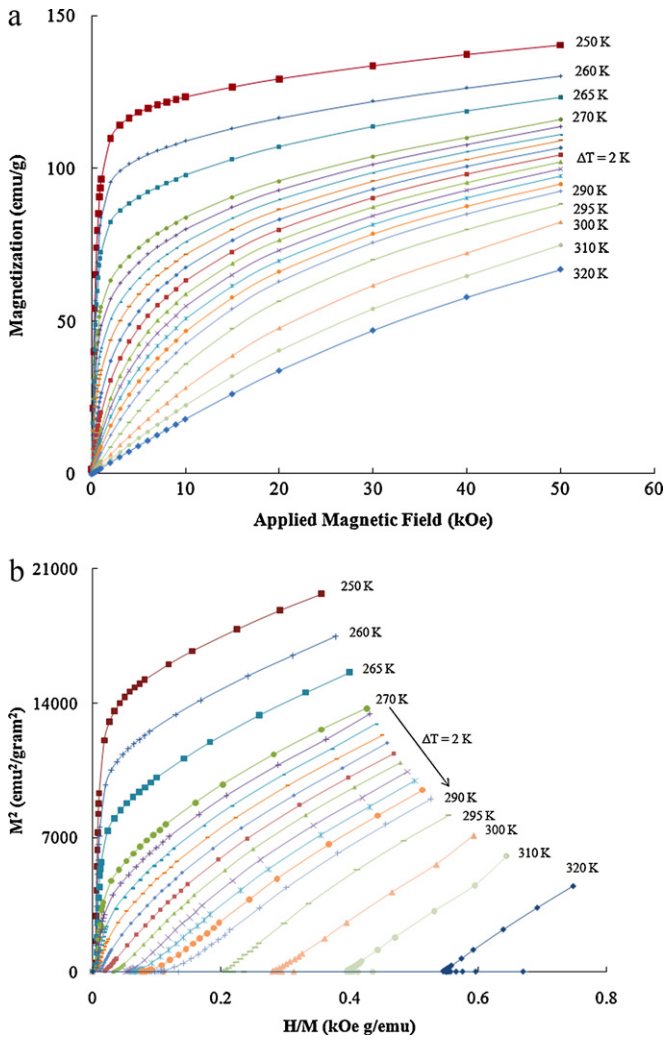

Fig. 6. (a) The isothermal magnetization curves near the transition temperature for as-cast $Gd_{90}Mn_{10}$ alloy. (b) Arrot plots for as-cast $Gd_{90}Mn_{10}$ alloy.

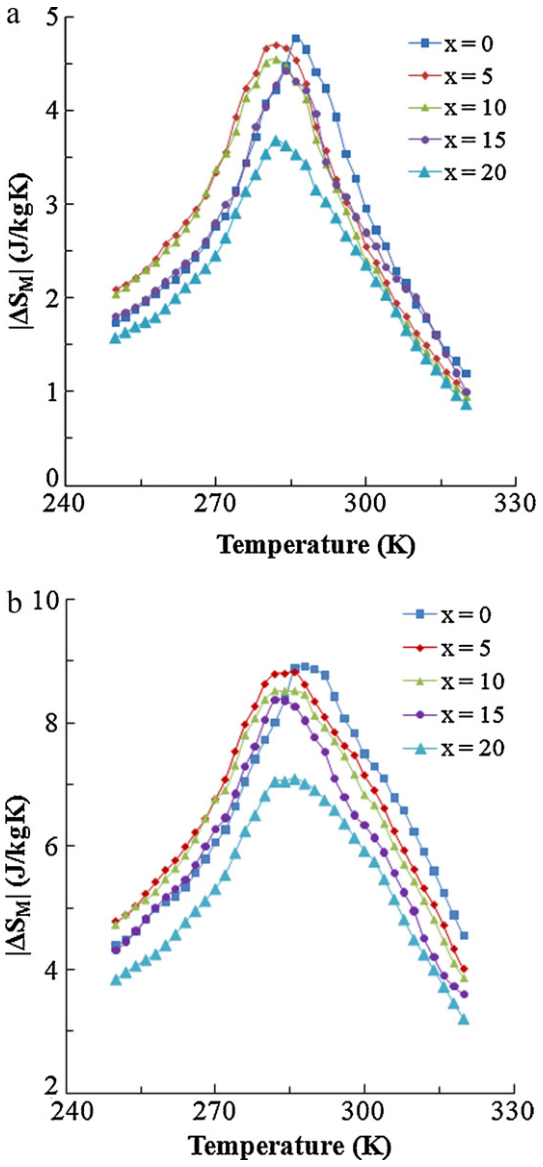

Fig. 7. The temperature dependence of magnetic entropy change ($|S_M|$) in as-cast $Gd_{100-x}Mn_x$ (x = 0, 5, 10, 15, 20 at.%) alloys obtained under a field change from: (a) 0 to 2 T. (b) 0 to 5 T.

for a particular alloy composition is due to the combined effect of variation of crystallographic orientation and composition of Mn among each grain. The average HVN (~200) for α-Gd phase for as-cast $Gd_{100-x}Mn_x$ (x = 5, 10, 15, 20) alloys is higher than the HVN for α-Gd phase in as-cast Gd (~140). The increase in HVN for α-Gd phase in as-cast $Gd_{100-x}Mn_x$ alloys as compared to as-cast Gd confirms solid solution strengthening of α-Gd phase. Similar values of HVN (~200) for α-Gd phase in as-cast $Gd_{100-x}Mn_x$ alloys confirms similar amount of Mn dissolved in α-Gd irrespective of their composition of Mn in the alloys. Thus the as-cast alloys viz. $Gd_{95}Mn_5$, $Gd_{90}Mn_{10}$, $Gd_{85}Mn_{15}$, and $Gd_{80}Mn_{20}$ having similar T_C (~279 K) values can be justified. T_C in Gd–Mn alloys could decrease further if increased amount of Mn forms substitutional solid-solution with α-Gd. Rapid solidification could be one possible way to increase the solubility of Mn in α-Gd.

The isothermal magnetization (M–H) curves were measured at various temperatures (250–320 K) around T_C. Fig. 6(a) shows such a curve for as-cast $Gd_{90}Mn_{10}$ alloy for 0–5 T as a representative. In the vicinity of the T_C, the temperature step is 2 K. The curves gradually change to straight lines above T_C suggesting gradual switch from ferromagnetic to paramagnetic state. Fig. 6(b) shows the Arrot plot [32] of as-cast $Gd_{90}Mn_{10}$ alloy for 0–5 T. The T_C (~279 K) values obtained from Arrot plot matches closely with the values obtained by the inflexion method. In the Arrot plots no 'S-sharp' curve appears and additionally no inflection or negative slope as an indication of metamagnetic transformation above T_C is observed which confirms the nature of the second order transition in as-cast Gd_{100-x}–Mn_x (x = 5, 10, 15, 20) alloys.

The magnetic entropy change ($|\Delta S_M|$) as a function of temperature and magnetic field for as-cast $Gd_{100-x}Mn_x$ (x = 0, 5, 10, 15, and 20 at.%) alloys were obtained from Eq. (2) using the magnetization measurements and the temperature and magnetic field dependence of magnetization. Fig. 7 shows the plot of $|\Delta S_M|$–T over the temperature range of 250–320 K for magnetic fields varying from 0 to 2 T (Fig. 7(a)) and 0 to 5 T (Fig. 7(b)). The $|\Delta S_M|$–T for as-cast $Gd_{100-x}Mn_x$ alloys show a 'caret-like' shape peaking at the Curie temperature typical for second order magnetic transitions, similar to earlier reports on Gd [4,33]. The $|\Delta S_M|_{max}$ for each of the alloy determined from the $|\Delta S_M|$–T curves (Fig. 6) for magnetic fields varying from 0 to 2 T and 0 to 5 T is listed in Table 1. The $|\Delta S_M|_{max}$ for as-cast Gd is 4.77 J/kg K and 8.92 J/kg K at magnetic fields varying from 0 to 2 T and 0 to 5 T, respectively which agrees with the previously reported values for arc-melted Gd [2–6,11,13]. For as-cast $Gd_{100-x}Mn_x$ alloys the $|\Delta S_M|_{max}$ decreases from 4.77 J/kg K ($Gd_{100}Mn_0$) to 3.67 J/kg K ($Gd_{80}Mn_{20}$) at mag-

netic fields varying from 0 to 2 T with an increase in Mn content. $|\Delta S_M|_{max}$, at magnetic fields varying from 0 to 5 T, decreases from 8.92 J/kg K ($Gd_{100}Mn_0$) to 7.10 J/kg K ($Gd_{80}Mn_{20}$) with an increase in Mn content. The values of $|\Delta S_M|_{max}$ are 4.69, 4.54, and 4.41 J/kg K for $Gd_{95}Mn_5$, $Gd_{90}Mn_{10}$, and $Gd_{85}Mn_{15}$, respectively at magnetic field varying from 0 to 2 T and the values of $|\Delta S_M|_{max}$ are 8.83, 8.52, and 8.38 J/kg K for $Gd_{95}Mn_5$, $Gd_{90}Mn_{10}$, and $Gd_{85}Mn_{15}$, respectively at magnetic field varying from 0 to 5 T. Such close values (differences less than 3%) of $|\Delta S_M|_{max}$ suggests negligible decrease in $|\Delta S_M|_{max}$ for as-cast $Gd_{100-x}Mn_x$ ($0 \le x \le 15$ at.%) and for all practical purpose the $|\Delta S_M|_{max}$ can be assumed to be constant (~4.6 J/kg K and ~8.6 J/kg K) at magnetic fields varying from 0 to 2 T and 0 to 5 T, respectively. However the differences in $|\Delta S_M|_{max}$ for as-cast $Gd_{85}Mn_{15}$ alloy and as-cast $Gd_{80}Mn_{20}$ alloy is appreciable (greater than 15%).

The refrigerant capacity (q) of as-cast $Gd_{100-x}Mn_x$ alloys was deduced numerically by integrating the area under the $|\Delta S_M|$–T curves using Eq. (3). The q for each of the alloy for magnetic fields varying from 0 to 2 T and 0 to 5 T is listed in Table 1. The q for as-cast Gd is 198 J/kg and 461 J/kg at magnetic fields varying from 0 to 2 T and 0 to 5 T, respectively which agrees with the previously reported values for Gd [2–6,11,13]. The q for as-cast Gd, $Gd_{95}Mn_5$, $Gd_{90}Mn_{10}$, and $Gd_{85}Mn_{15}$ alloys show no appreciable change (~195 J/kg and ~450 J/kg at magnetic fields varying from 0 to 2 T and 0 to 5 T, respectively). However there is appreciable decrease (~20%) in q for as-cast $Gd_{80}Mn_{20}$ alloy (~163 J/kg K and ~ 376 J/kg K at magnetic fields varying from 0 to 2 T and 0 to 5 T as compared to other composition of as-cast alloys. Replacing less than ~15 at.% of Gd with Mn does not change q appreciably in as-cast Gd–Mn alloys which suggests that these alloys could be less expensive material to start with in finding improved MCE in SOT materials based on Gd alloys.

In the present study we observe T_C for as-cast $Gd_{100-x}Mn_x$ (x = 5, 10, 15 and 20 at.%) alloys is less than as-cast Gd which is similar to the trend observed in the case of as-cast Gd–V, melt-spun Gd–Co and as-cast Gd–Zn alloys [12,16,17]. In the conventionally melted Gd_{100-x}–V_x alloys ($0 < x \le 10$) T_C (~290 K) decreases by ~3 K as compared to as-cast Gd [17] and in the conventionally melted $Gd_{100-x}Zn_x$ alloys ($0 < x \le 20$) have T_C (~270 K) decreases by ~23 K as compared to as-cast Gd [16]. However in the as-cast Gd_{100-x}–Mn_x ($0 < x \le 15$) alloys T_C (~280 K) decreases by ~13 K as compared to as-cast Gd. The alloying of Gd with a non-magnetic (diamagnetic/paramagnetic) transition element in 4th Period of the Periodic Table decreases the T_C of Gd and the decrease in T_C seem to increase as one moves across the Period (from Sc to Zn). It may be noted that the melt-spun $Gd_{100-x}Co_x$ alloys ($0 < x \le 30$) alloys have T_C ~ 198 K which is ~100 K less than Gd. The combined effect of presence of finer microstructure of α-Gd having greater dissolved Co and amorphous phases due to rapid solidification decreases T_C by ~100 K. Relatively faster cooling of the as-cast $Gd_{100-x}Mn_x$ (x = 5, 10, 15 and 20 at.%) alloys compared to the one in the present work could probably decrease the T_C and hence their working temperature could be increased. The $|\Delta S_M|_{max}$ and q increases for Gd–V alloys but decreases for Gd–Zn alloys. However the present study shows appreciably small changes in the $|\Delta S_M|_{max}$ and q for $Gd_{100-x}Mn_x$ ($0 < x \le 15$) alloys and this behavior is similar to that observed in melt-spun Gd–Co alloys, as-cast Gd–Y and Gd–Yb alloys [2,18]. The near constant values of the $|\Delta S_M|_{max}$ and q values coupled with ~13 K decrease T_C for as-cast $Gd_{100-x}Mn_x$ alloys, as compared to Gd, suggests expansion of the working temperature region of Gd upon alloying with Mn up to ~15 at.%. This makes less expensive Gd–Mn alloys potential candidates (similar to Gd–Co, Gd–Y and Gd–Yb alloys) as composite magnetic refrigerant materials working near room temperature in an Ericsson cycle. In an ideal Ericsson cycle consisting of two isothermal and two isofield steps the requirement of constant $|\Delta S_M|$ provides optimal performing conditions [2]. Low cost, tunable T_C, and favorable MCE properties make $Gd_{100-x}Mn_x$ ($0 < x \le 15$) potential candidates as SOT based magnetic refrigerants for near room temperature applications.

4. Conclusions

A series of $Gd_{100-x}Mn_x$ (x = 0, 5, 10, 15, and 20 at.%) alloys were prepared by arc-melting. The X-ray spectra and optical metallography show that the as-cast alloys were comprised of α-Gd and $GdMn_2$ phase. With the increase in Mn content the amount of α-Gd phase decreased while $GdMn_2$ phase increased. A decrease in T_C (~279 K) values for the as-cast alloys (x = 5, 10, 15, and 20 at.%) as compared to as-cast Gd (~292 K) was observed. Similar values of T_C for these alloys suggest the presence of similar amounts of Mn in α-Gd forming substitutional solid-solution, which is supported by similar Vickers microhardness values for the as-cast alloys. At any temperature the magnetization values for the as-cast alloys decreases with the increase in at.% of Mn owing to increase in 'non-magnetic' $GdMn_2$ phase and decrease in ferromagnetic α-Gd phase. The $|\Delta S_M|_{max}$–T curves shows no appreciable decrease in the $|\Delta S_M|_{max}$ values ~4.6 J/kg K (0–2 T) and ~8.6 J/kg K (0–5 T) upon alloying Mn with Gd up to $x \le 15$ at.%. Refrigerant capacity (q) showed negligible variation ~195 J/kg (0–2 T) and 450 J/kg (0–5 T) with increasing Mn ($x \le 15$ at.%) content. Near constant values of $|\Delta S_M|_{max}$ and q coupled with ~13 K decrease in T_C for as-cast $Gd_{100-x}Mn_x$ alloys as compared to Gd, suggests expansion of working temperature region of Gd upon alloying with Mn up to 15 at.%. The as-cast $Gd_{100-x}Mn_x$ ($0 \le x \le 15$) alloys may be used as layered structures of magnetic refrigerants to obtain broader region of magnetic entropy change. Adjustable T_C, favorable properties of MCE make $Gd_{100-x}Mn_x$ ($0 \le x \le 15$) alloys potential candidates as second-order transition based magnetic refrigerants for near room temperature air-conditioning and magnetic refrigeration.

Acknowledgment

This work was supported by National Science Foundation Grant Nos. DMR-0504706 and 0840407.

References

[1] E. Warburg, Ann. Phys. (Leipzig) 13 (1881) 141.
[2] A.M. Tishin, Y.I. Spichkin, The Magnetocaloric Effect and its Applications, Institute of Physics Publishing, Bristol and Philadelphia, 2003.
[3] G.V. Brown, J. Appl. Phys. 47 (8) (1976) 3673.
[4] K.A. Gschneidner Jr., V.K. Pecharsky, Annu. Rev. Mater. Sci. 30 (2000) 387.
[5] K.A. Gschneidner Jr., V.K. Pecharsky, Mater. Sci. Eng. A 287 (2000) 301.
[6] A.M. Tishin, K.H.J. Buschow (Eds.), Handbook of Magnetic Materials, vol. 12, Elsevier Science, The Netherlands, 1999 (Chapter 4).
[7] O. Tegus, E. Bruck, K.H.J. Buschow, F.R. de Boer, Nature 415 (2002) 150.
[8] V.K. Pecharsky, K.A. Gschneidner Jr., J. Magn. Magn. Mater. 167 (3) (1997) L179.
[9] H. Wada, Y. Tanabe, Appl. Phys. Lett. 79 (2001) 3302.
[10] F.X. Hu, B.G. Shen, J.R. Sun, Z.H. Cheng, G.H. Rao, X.X. Zhang, Appl. Phys. Lett. 78 (2001) 3675.
[11] V.K. Pecharsky, K.A. Gschneidner Jr., Ya Mudryk, Durga Paudyal, J. Magn. Magn. Mater. 321 (21) (2009) 3541.
[12] C.L. Zhang, D.H. Wang, Z.D. Han, H.C. Xuan, B.X. Gu, Y.W. Du, J. Appl. Phys. 105 (2009) 013912.
[13] K.A. Gschneidner Jr., V.K. Pecharsky, A.O. Tsokol, Rep. Prof. Phys. 68 (2005) 1479.
[14] E. Bruck, O. Tegus, D.T.C. Thanh, K.H.J. Buschow, J. Magn. Magn. Mater. 310 (2) (2007) 2793.
[15] C.D. Fuerst, J.F. Herbst, R.K. Mishra, R.D. McMichael, J. Appl. Phys. 76 (10) (1994).
[16] V.K. Pecharsky, K.A. Gschneidner Jr. (Eds.), Cryocoolers, vol. 10, Academic/Plenum Publishers, 1999.
[17] Z. Feng, W. Wu, H. Zhao, Y. Gangfu, Rare Met. Mat. Eng. 38 (2009) 1378.
[18] S. Kito, H. Nakagome, T. Kobayashi, A.T. Saito, H. Tsuji, in: S.D. Miller, R.G. Ross (Eds.), Cryocoolers 14, International Cryocoolers Conference Inc. Boulder, CO, 2007.
[19] W. Dunhui, H. Songling, H. Zhida, S. Zhenghua, W. Yi, D. Youwei, Solid State Commun. 131 (2004) 97.
[20] W. Dunhui, H. Songling, H. Zhida, S. Zhenghua, W. Zou, D. Youwei, J. Alloys Compd. 387 (2005) 6.

[21] S.G. Min, K.S. Kim, S.C. Yu, H.S. Suh, S.W. Lee, J. Magn. Magn. Mater. 303 (2006) e440.
[22] D. Wang, S. Huang, Z. Han, Z. Su, W. Zou, Y. Du, J. Alloys Compd. 377 (2004) 72.
[23] Q.Y. Dong, B.G. Shen, J. Chen, J. Shen, H.W. Zhang, J.R. Sun, J. Appl. Phys. 105 (2009) 07A305.
[24] B.J. Chevalier, L. Bobet, M. Nakhl, J. Etourneau, J. Alloys Compd. 320 (2001) 33.
[25] J. Sanchez Marcos, J. Rodriguez Fernandez, B. Chevaliar, J.L. Bobet, J. Etourneau, J. Magn. Magn. Mater. 272–276 (2004) 579–580.
[26] H. Okamoto, in: H. Okamoto, P.R. Subramanian, L. Kacprzak (Eds.), Binary Alloy Phase Diagrams, vol. 2, ASM International, Materials Park, OH, 1992, p. 1897.
[27] H. Okamoto, J. Phase Equilibr. Diffus. 23 (5) (2002) 459.
[28] B. Ouladdiaf, C. Ritter, R. Ballou, J. Deportes, Phys. B 276–278 (2000) 670.
[29] Gunter Petzow, Metallographic Etching, 2nd ed., ASM International, 2003.
[30] Metals-Mechanical Testing, Annual Book of ASTM Standards 03. 01, 2005, p. 438.
[31] S. Chaudhary, V.S. Kumar, S.B. Roy, P. Chaddah, S.R. Krishnakumar, V.G. Sathe, A. Kumar, D.D. Sarma, J. Magn. Magn. Mater. 202 (1999) 47.
[32] A. Arrot, Phys. Rev. 108 (1957) 1394.
[33] A.L. Lima, K.A. Gschneidner Jr., V.K. Pecharsky, J. Appl. Phys. 96 (4) (2004) 2164.